Renewable Energy 169 (2021) 1242–1251

Contents lists available at ScienceDirect

Renewable Energy

journal homepage: www.elsevier.com/locate/renene

Macro-kinetic model for CuO–ZnO–ZrO_2@SAPO-11 core-shell catalyst in the direct synthesis of DME from CO/CO_2

Ainara Ateka *, Ander Portillo , Miguel Sánchez-Contador , Javier Bilbao , Andres T. Aguayo

Chemical Engineering Department, University of the Basque Country UPV/EHU, Box 644, 48080, Bilbao, Spain

ARTICLE INFO

Article history:
Received 28 October 2020
Received in revised form
7 January 2021
Accepted 9 January 2021
Available online 14 January 2021

Keywords:
Kinetic model
DME synthesis
Core-shell catalyst
CO_2 conversion
Deactivation

ABSTRACT

An original kinetic model has been used to describe the performance of an original CuO–ZnO –ZrO_2@SAPO-11 bifunctional catalyst on the one-stage synthesis of dimethyl ether (DME) from CO/CO_2 hydrogenation. The model considers that certain individual reactions (the synthesis of methanol and the reverse water gas shift) occur in the metallic function (core) of the catalyst particle, whereas others (methanol dehydration) take place in the shell (acid function), and that the progress of these reactions is conditioned by the diffusion of the components. The kinetic parameters of the individual reactions and the deactivation kinetics have been calculated from experimental data obtained in a wide conditions range (H_2/CO_x ratio, 2.5–4; CO_2/CO_x ratio, 0–1; 10–50 bar; 250–325 °C; 1.25–20 g h mol_C^{-1}). The use of the model for simulating the packed bed reactor has allowed evaluating the influence of the reaction conditions, as well as assessing the effect of the catalysts particle size. The model predicts DME yields of 64% for syngas (H_2+CO) feeds, 38% for CO_2/CO_x ratio of 0.50 and 17% for H_2/CO_2, respectively, at 70 bar and 290 °C. The maximum conversion of CO_2 predicted by the model for the same space time value and temperature surpasses 30% for H_2+CO_2 feedstocks at 70 bar, greater than the experimental value obtained at 50 bar at the same temperature (~25%).

Abbreviations.

CO_x	CO + CO_2 mixture
CS	Core-shell
DME, HC, MeOH	Dimethyl ether, hydrocarbons and methanol, respectively

Greek symbols.

$\Delta H_{ads,i}$, $\Delta H^d_{ads,i}$,	Term associated to the adsorption heat of *i* component at zero TOS and deactivation kinetics, kJ mol^{-1}
β	kinetic constant for paraffins formation, mol_{HC} g^{-1} h^{-1}
ρ	Catalyst particle density, g m^{-3}
θ_i	Term for quantifying the attenuation of the reaction rates by component *i* (being i H_2O and/or CO_2)
θ_d	Term for quantifying the attenuation of the deactivation rate

1. Introduction

CO_2 capture, utilization and storage technologies (CCUS) have to face the pressing challenge of halting climate change and ocean acidification [1]. The severity of the problem is evident with the forecast of fossil fuels use predicted in 2019 by the International Energy Agency (IEA) [2] and the continuous increase of CO_2 concentration in the atmosphere (from 409 ppm in 2019 to 450 ppm in 2035) [3]. In this regard, the valorization of CO_2 is also an opportunity to use an abundant carbon source. However, the selection of the most appropriate valorization strategy is a complex issue, due to the multitude of alternatives and the economic and environmental constraints for their implementation [4].

Among the CO_2 valorization routes, thermal catalytic conversion (hydrogenation) into fuels and chemicals is the most attractive for producing methanol, methane, dimethyl ether (DME), olefins, aromatics or gasoline [5]. It is overall considered that the use of renewable energies is required for the viability of the proposed processes, in particular for the generation of the H_2 required [6,7]. Some of the catalytic processes for valorizing CO_2, such as the synthesis of methanol and hydrocarbons (Fischer-Tropsch (FT)

* Corresponding author.
E-mail address: ainara.ateka@ehu.eus (A. Ateka).

https://doi.org/10.1016/j.renene.2021.01.062
0960-1481/

Nomenclature

D	Reactor diameter, m
d	Deactivation order
$D_{e,i}$	Coefficient for the effective diffusion, $m^2\ h^{-1}$
dp	Catalyst particle size diameter, m
$F^0_{CO_2}, F_{CO_2}$	CO_2 molar flow rate at the reactor inlet and outlet, respectively, $mol_C\ h^{-1}$
$F^0_{CO_x}, F_{CO_x}$	$CO + CO_2$ molar flow rate at the reactor inlet and outlet, respectively, $mol_C\ h^{-1}$
F_i	Carbon molar flow rate of component *i* at the reactor outlet, $mol_C\ h^{-1}$
f_i	Fugacity of component *i*, bar
$K_{ads,\ CO_2}, K_{ads,H_2O}$	Adsorption equilibrium constant related to reaction rate attenuation by CO_2 or H_2O, respectively, bar^{-1}
$K^d_{ads,CO_2}, K^d_{ads,H_2O}$	Adsorption equilibrium constant related to deactivation rate limitation by CO_2 or H_2O, respectively, bar^{-1}
k_d	Kinetic constant for deactivation, $bar^{-1}\ h^{-1}$
K_j	Equilibrium constant of *j* reaction step
k_j	Kinetic constant of *j* reaction step
L	Reactor length, m
n_i	Carbon atoms in compound *i*
P	Total pressure, bar
R	Radius of the particle, m
r	Radial position in the particle
r_d	Deactivation rate, h^{-1}
r_i	Component *i* formation rate, $mol_C\ g^{-1}\ h^{-1}$
r_j	Reaction rate of *j* reaction step
T, T*	Temperature and reference temperature, respectively, K
t	Time, h
TOS	Time on stream, h
V_m	VTotal Micropore and total pore volume, respectively, cm^3g^{-1}
X_{CO_2}	Conversion of CO_2, %
Y_i	Yield for component *i*, %
y_i	Molar fraction of component *i*, in C units
$y_{i,\ ext}$	Molar fraction of component *i* in the gas surrounding the particle, in C units

synthesis) are based on well-developed technologies using syngas as feedstock. The studies on CO_2 valorization (directly or when co-fed together with syngas) in these processes have focused on tailoring and modifying the catalysts and the reaction conditions [8].

The high energy requirements and CO_2 emissions of the current routes for olefins production (steam or catalytic cracking of oil derivates) justifies the interest of replacing these routes by others, with CO_2 as raw material [9,10]. In this regard, modifying the FT catalyst (generally Fe supported) by incorporating an acid function (HZSM-5 zeolite or SAPO-34) facilitates light olefins selectivity, through the cracking of higher hydrocarbons formed as intermediates [11]. Another attractive route for production of light olefins from CO_2, consists of incorporation of an acid function (SAPO-34 is the most studied) to methanol synthesis metallic catalysts (based on CuO–ZnO). In this case, the production of light olefins takes place through the dual cycle mechanism [12], with methanol as an intermediate (OX-ZEO concept) [13–16]. The OX-ZEO concept also allows for producing aromatics selectively from CO_2 using ZnO–ZrO_2 and HZSM-5 catalysts [17].

The aforementioned CO_2 valorization processes have thermodynamic limitations (methanol synthesis), lack of selectivity (conventional FT) or lack of technological maturity for their industrial application (modified FT or OX-ZEO synthesis). Given these limitations, the one-stage DME synthesis offers thermodynamic and economic advantages over methanol synthesis for CO_2 valorization [18,19]. Besides, catalysts preparation and reactor design have achieved a significant technological development for this process [20–24].

The reactions involved are as follows:

$$CO + 2H_2 \leftrightarrow CH_3OH \quad (1)$$

$$CO_2 + 3H_2 \leftrightarrow CH_3OH + H_2O \quad (2)$$

$$CO_2 + H_2 \leftrightarrow CO + H_2O \quad (3)$$

$$2CH_3OH \leftrightarrow CH_3OCH_3 + H_2O \quad (4)$$

$$CO + 3H_2 \leftrightarrow CH_4 + H_2O \quad (5)$$

Accomplishing the dehydration of methanol in the same reactor (Eq. (4), catalyzed by the acid function) displaces methanol synthesis reactions equilibrium (Eq. (1) and (2), catalyzed together with the rWGS (Eq. (3)) by the metallic function) and favors the conversion of CO_2 [25,26]. This reaction of methanol conversion to DME occurs following a mechanism with methoxy ions as intermediates. The mechanism can be dissociative [27] or associative [28], and its progress is conditioned by the acidity of the catalyst and to a greater extent by its porous structure [29].

Furthermore, DME has various commercial applications, as aerosol, coolant, household and automotive fuel [30] and as H_2 source [31]. Besides, DME is an attractive alternative for replacing methanol as raw material for producing olefins or aromatics, due to its greater reactivity [32–34]. For the DTO process (DME to olefins), a reactor-regenerator system has been proposed, similar to that used industrially in the MTO process [35].

The preparation of catalysts for this reaction has received particular attention [22,36], being the enhancement of their selectivity and stability priority objectives. The sintering of the Cu^0 sites may be attenuated by using promoters (ZnO, Al_2O_3, CeO_2, MgO, ZrO_2, MnO) [37–43]. The formation of coke in the acid function (being γ-Al_2O_3 and HZSM-5 the most used ones) is attenuated by passivating the strong acid sites [44] and decreasing zeolites crystal size [45]. It should be noted that the formation of coke is mitigated when CO_2 is co-fed with. This result is associated to the high H_2O concentration in the medium (generated mainly by the rWGS reaction (Eq. (3)) [46–48].

An initiative to increase DME production is the preparation of a bifunctional CuO–ZnO–ZrO_2@SAPO-11 catalyst with a core-shell configuration. In previous works [49,50] the high stability, activity and selectivity of this catalyst were ascertained. Previously, the preparation conditions and the adequate ZrO_2 content in the metallic function were established [51]. Besides, the good behavior of SAPO-11 was also studied as to minimize side reactions of coke formation [52]. The higher DME yield obtained using the core-shell catalyst with respect to the hybrid catalyst with the same composition is explained by the detachment of the individual reactions (Eqs. (1)–(5)) in two regions of the particle. Thus, methanol synthesis and rWGS reactions (Eq. (1), (2) and (3), respectively) take place in the metallic function (core), whereas methanol dehydration

(Eq. (4)) occurs in the acid function (shell), and the undesired formation of CH_4 (Eq. (5)) takes place in both functions. The greater reactivity of CO over CO_2 is well established in both methanol and FT synthesis [53] and the fast separation of H_2O from the metallic function (CuO–ZnO–ZrO_2) facilitates the formation of CO (Eq. (3)). Furthermore, the location of the reactions facilitates a homogeneous circulation of the reaction components in each catalyst particle, avoiding the distribution of contact time with the active sites of each function, which lead to undesirable reactions. The influence of the preparation on the properties of each function must also be considered. Thus, the preparation of the core-shell particles avoids partially blocking the SAPO-11 pores by the CuO–ZnO–ZrO_2 particles as it occurs when preparing a hybrid catalyst by pelletization of the functions [49]. This difference in the porous structure will facilitate the progress of the methanol dehydration mechanism, since it is conditioned by the porous structure [29].

The bifunctional core-shell catalysts has previously been studied for the syngas to DME process (STD), with Cr_2O_3–ZnO@SAPO-46 [54], CuO–ZnO–Al_2O_3@SiO_2–Al_2O_3 [55], or CuO–ZnO–Al_2O_3@SAPO-11 [56] catalyst. Das et al. [57] made a review on the performance of core-shell catalysts in alternative processes (electrocatalytic, thermocatalytic and others) for CO_2 conversion into syngas and valuable hydrocarbons.

Here, a macrokinetic model has been developed for DME synthesis over a CuO–ZnO–ZrO_2@SAPO-11 catalyst. The model considers that the individual reactions (Eqs. (1)–(5)) occur in two separate regions of the catalyst particle and also that their reaction rates are conditioned by the internal diffusion of the reactants. The macrokinetic model has been used for simulating the reactor for a parametric study of the hydrogenation of CO and CO_2 mixtures, and for simulating the performance of the catalyst prepared with different diffusion restrictions, such as those inherent to a bigger particle size, as required for its use at larger reaction scale. In this comparison, DME yield and the conversion of CO_2 have been studied, as two complementary targets due to their economic and environmental interest, respectively. The proposed model is a useful tool for simulating the process in reactors using this catalyst. Indeed, it is based on general criteria, applicable to describe the behavior of other bifunctional core-shell catalysts in this and other catalytic processes.

2. Experimental

2.1. Catalyst

The catalyst, denoted as CZZr@S-11 hereafter, was prepared by coating the CuO–ZnO–ZrO_2 function cores with the SAPO-11 in a 1/2 mass ratio. Ludox TMA-34 silica solution was used as adhesive. For this, first, the metallic cores (90–120 μm) were prepared by Cu, Zn and Zr nitrates (1 M) co-precipitation with Na_2CO_3 and thermally treated at 300 °C (10 h). The SAPO-11 was synthesized in a laboratory scale Teflon coated autoclave at 195 °C (24 h), from a H_3PO_4, Disperal and Ludox AS-40, using di-propylamine as template and was thermally treated at 575 °C. Once the individual functions were obtained, the metallic cores were moisturized with the adhesive and the acid function was added to form the shell of the particle. The resulting particles were dried and thermally treated at 400 °C (2 h), and sieved to 125–800 μm particles. The preparation methodology and the selection of the individual functions conforming the catalyst (attending to their good catalytic performance) have been detailed in previous works [49,51,52].

The catalysts were characterized using various techniques described in detail elsewhere [49,51,52] and summarized in S1 section of the Supporting Information. Table 1 gathers the most relevant results derived from these analyses.

Besides, the physical properties, thus, density and porosity, may have a relevant influence on the kinetic behavior of the catalyst. In this regard, the porosity is required to quantify the effective diffusion coefficient in the particle. This parameter was determined by Hg intrusion porosimetry in an Autopore 9220 equipment (Micromeritics). To avoid the reaction of Hg with the Cu in the catalyst, the study was carried out using a catalyst prepared without Cu, that is, with ZnO–ZrO_2 as metallic function encapsulated in SAPO-11 (for the core-shell configuration) following the usual procedure previously described. According to the results in Fig. 1, the existence of macropores with a diameter in the 0.1–0.4 μm range is predominant, which is attributable to the metallic phase. As a result, the average macropore diameter and the porosity are significant (0.20 μm and 0.76, respectively). The density of the catalyst particles is 0.615 g ml^{-1}.

2.2. Reaction equipment, conditions and indices

The activity tests were conducted in a reaction equipment previously described elsewhere [49,50]. To assure isothermal conditions, the catalyst was diluted in SiC (inert solid). The catalyst was subjected to a H_2 flowrate (at 250 °C) prior to each run for reducing the CuO species resulting from calcination to the active Cu^0 species.

The reaction condition ranges used for the study were: H_2/CO_x molar ratio between 2.50 and 4.0; CO_2/CO_x molar ratio between 0 and 1; 250–325 °C; 10–50 bar; space time, below 20 g_{cat} h mol_C^{-1}; time on stream (TOS) up to 48 h.

The studied reaction indices are as follows:

Yields of DME and methanol (as byproduct): $Y_i = \frac{n_i F_i}{F^0_{COx}} 100$ (6)

$$\text{Conversion of } CO_2{:}X_{CO_2} = \frac{F^0_{CO_2} - F_{CO_2}}{F^0_{CO_2}} \ 100 \qquad (7)$$

where F^0_{COx} and $F^0_{CO_2}$ represent the molar flow rates of CO_x ($CO + CO_2$) and CO_2 in the reactor inlet and F_i is the molar flowrate of i component at the outlet stream. n_i refers to the carbon atoms contained in each molecule.

Positive value of X_{CO2} means that a net valorization of the CO_2 (fed and formed by the WGS reaction (Eq. (3)) has been accomplished, that is, avoiding a net formation of CO_2 in the process, which correspond to negative values of X_{CO_2}.

3. Macrokinetic model description

The kinetic model considers that the reactions of methanol synthesis and rWGS occur in the core region of the particle catalyzed by the CuO-ZnO-ZrO_2 function (Fig. 2); while methanol dehydration to DME occurs in the shell region, catalyzed by the SAPO-11. The side reaction of paraffins formation (being CH_4 the main product, with very low yield) takes place in both regions, that is, in the core through Fischer-Tropsch and methanation reactions, and in the shell following the dual cycle mechanism [12], initially forming light olefins, which are later hydrogenated to paraffins.

The rates of each reaction are described by the following kinetic equations (previously used to establish an apparent kinetic model [53]):

Methanol synthesis from CO and CO_2:

$$r_{MeOH} = \left[k_1 \left(f^2_{H_2} f_{CO} - \frac{f_{CH_3OH}}{K_1} \right) + k_4 \left(f^3_{H_2} f_{CO_2} - \frac{f_{CH_3OH} f_{H_2O}}{K_4} \right) \right] \theta_{H_2O} \ a \qquad (8)$$

where:

Table 1
Properties of the catalyst.

Textural properties			Metallic properties			Acidic properties	
S_{BET} ($m^2\ g^{-1}$)	V_m ($cm^3\ g^{-1}$)	V_{total} ($cm^3\ g^{-1}$)	S_{Cu} ($m^2 g_{Cu}^{-1}$)	S'_{Cu} ($m^2 g_{catalyst}^{-1}$)	Disp. (%)	Total acidity ($mmol_{NH3} g^{-1}$)	Av. Acid strength ($kJ\ mol_{NH3}^{-1}$)
123	0.031	0.300	33.3	3.9	5.1	0.186	85

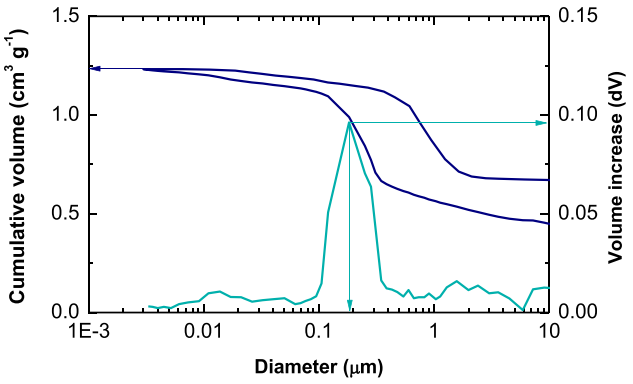

Fig. 1. Hg porosimetry for catalyst.

$$\theta_{H_2O} = \frac{1}{1 + f_{H_2O} K_{ads,H_2O}} \tag{9}$$

$$\text{Methanol dehydration: } r_{DME} = k_2 \left[f_{CH_3OH}^2 - \frac{f_{CH_3OCH_3} f_{H_2O}}{K_2} \right] a \tag{10}$$

$$\text{WGS reaction: } r_{WGS} = k_3 \left[f_{H_2O} f_{CO} - \frac{f_{CO_2} f_{H_2}}{K_3} \right] \theta_{CO_2} a \tag{11}$$

where:

$$\theta_{CO_2} = \frac{1}{1 + f_{CO_2} K_{ads,CO_2}} \tag{12}$$

$$\text{Paraffins formation: } r_{HC} = \beta \tag{13}$$

The deactivation of the catalyst is quantified in Eqs. (8), (10) and (11) with the activity, a, defined as:

$$a = \frac{r_i}{(r_i)_0} \tag{14}$$

where r_i and $(r_i)_0$ are the formation rates or methanol, DME or CO_2 at t and at zero TOS, respectively.

The deactivation kinetic equation is:

$$-\frac{da}{dt} = k_d (f_{MeOH} + f_{DME}) \theta_d \ a^d \tag{15}$$

$$where: \quad \theta_d = \frac{1}{1 + f_{H_2O} K_{ads,H_2O}^d + f_{CO_2} K_{ads,CO_2}^d} \tag{16}$$

It should be noted that the reaction rate in the synthesis of methanol (Eq. (8)) is considered to be conditioned by the competitive adsorption of H_2O, and the rate of the WGS reaction (Eq. (11)) is considered to be conditioned by the adsorption of CO_2. On the other hand, the rate of paraffins formation is quantified by a constant (Eq. (13)), β, and catalyst deactivation kinetics (Eq. (16)) is considered to be attenuated by the adsorption of both H_2O and CO_2.

The macrokinetic model considers the diffusional limitation of the reactants in each region of the catalyst particle. The concentration (molar fraction, y_i) profile of each component i is determined by the expression of the mass balance (considering spherical geometry) [58–61]:

$$D_{e,i} \left(\frac{d^2 y_i}{dr^2} + \frac{2}{r} \frac{dy_i}{dr} \right) = r_i \rho \tag{17}$$

where D_{ei} is its effective diffusion coefficient, r the radial coordinate, and ρ its density.

Considering the core-shell structure (Fig. 2), the model establishes for the core (metallic function) Eq. (17) for the reactions of methanol synthesis, r_{WGS} and paraffins formation with the kinetic equations described in Eqs. (8), (11) and (13), along with the deactivation equation in Eq. (15). To consider methanol diffusion through the metallic function, the reaction term has not been considered in equation Eq. (17). The boundary conditions of these equations in the core region are the following:

$$for\ r = 0 \quad \frac{dy_i}{dr} = 0 \tag{18}$$

$$for\ r = r_c \quad D_{e,i} \frac{dy_i}{dr^-} = D_{e,i} \frac{dy_i}{dr^+} \tag{19}$$

The mass conservation equations in the shell region of the particle (acid function) are established using Eq. (17) with the kinetic equation for methanol dehydration (described in Eq. (10)) and paraffins formation (with the kinetic equation described in Eq.

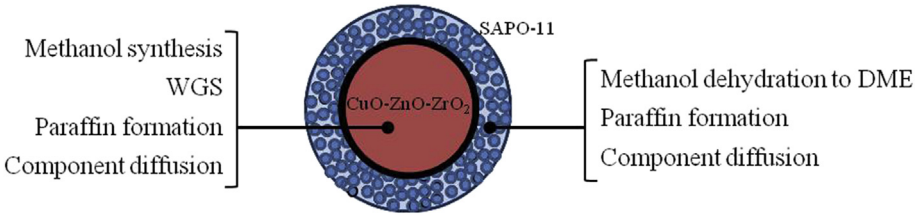

Fig. 2. Reactions considered in each region of the catalyst particle in the macrokinetic model.

(13)). In this region CO and CO_2 diffusions are considered in Eq. (17) without reaction of these components.

The boundary conditions in the shell region are therefore: Eq. (19) for $r = r_c$, and:

for $r = R$

$$y_{i,R} = y_{i,ext} \tag{20}$$

where $y_{i,ext}$ refers to the component i in the surrounding gas.

The calculation of the effective diffusion ($D_{e,i}$) of each component i through the catalyst is explained in Section S2 of the Supporting Information, along with the properties of the catalyst in the calculation.

4. Model and kinetic parameters

A program has been developed using Matlab software to solve the macrokinetic model (Fig. S3). The program collects the following data: i) values of the operating variables (feedstock composition, pressure, temperature, space time, and TOS); ii) experimental results of components molar fraction at the reactor outlet for the multiple operating conditions tested; iii) diffusion coefficient of each component through the catalyst. Next, the differential equations of the components formation kinetics are integrated together with the mass conservation equations with an integration subroutine developed for this specific purpose. This subroutine uses the ODE15S function of Matlab for integrating the differential equations along the catalyst particle (radial profile). Additionally, the subroutine also solves the mass conservation equations in the longitudinal profile of the reactor. Dispersive gas flow has been considered in the equivalent set of 16 CSTR in series. These number of equivalent stages (16) has been determined from the L/D (reactor length to diameter) and L/dp (reactor length to catalyst particle diameter) ratios according to the criteria established by Fogler [62]. In each of the equivalent CSTR the evolution with TOS of the composition for all the components has been calculated in n sections of the catalyst particle and in the gas surrounding it. In this way the program calculates the radial profile of each components concentration in the catalyst particle and the longitudinal profile along the fixed-bed reactor, together with catalyst activity and components concentrations. The methodology for analyzing the kinetic data and optimizing the fitting of the calculated concentration results to the experimental values has been detailed in a previous work on the calculation of an apparent kinetic model [53].

The equilibrium constants of the reaction steps (K_j) has been calculated as a function of temperature [26,63]. The kinetic constants and adsorption equilibrium constants have been reparameterized according to the relationship with temperature described in Eqs. (21) and (22), respectively.

$$k_j = k_j^* \exp\left[-\frac{E_j}{R}\left(\frac{1}{T}-\frac{1}{T^*}\right)\right] \tag{21}$$

$$K_{ads,i} = K_{ads,i}^* \exp\left[\frac{\Delta H_{ads,i}}{R}\left(\frac{1}{T}-\frac{1}{T^*}\right)\right] \tag{22}$$

The values of the effective diffusion coefficients of the components through the core-shell particles have been gathered in Table 2. The calculation of these parameters has been described in the Supporting Information section. A block diagram summarizing the resolution of the macrokinetic model is depicted in Fig. S6.

Table 3 lists the kinetic parameters (at the reference temperature of 275 °C) calculated for the reactions comprised in the kinetic scheme (Eqs. (1)–(5)).

As an illustration of quality of the results obtained with the model for different space time values are plotted in Fig. 3, and those for diverse CO_2/CO_x contents in the feed in Fig. 4. Graphs (a) and (b) correspond to DME and methanol yields, respectively, and graphs (c) to CO_2 conversion. The good prediction of the experimental results (symbols) obtained with the model (lines) is to be highlighted. In all operating conditions, a slight deactivation is observed in the first 10 h on stream and stabilizes after that period, maintaining almost constant DME and methanol yield and CO_2 conversion values.

The high DME yield (over 10% for 5 g h mol_C^{-1} and syngas feed (Fig. 4a)) and CO_2 conversion values (25% for H_2+CO_2 feeds, Fig. 4c) attained with this catalyst are attributed to the aforementioned effects of separating the individual reactions in the two regions (core and shell). Likewise, it is to be highlighted the stability for high CO_2 concentration feeds, and therefore at high H_2O concentration in the reaction medium. This feature of the catalyst allows for performing the reaction at 325 °C (Figs. S4 and S5) since the negative synergies derived from the contact between both functions are diminished. Thus, as determined in the literature for hybrid catalysts, the migration of Al^{3+} species of the acid function favor the sintering of Cu^0 crystals. The presence of H_2O also favors this feature [64–66]. As observed in Fig. 4 the higher CO_2 content in the feedstock enhances catalyst stability, resulting from the lessening of coke deposition due to the high concentration of H_2O [50]. The operating conditions that favor the yield of DME (Figs. 3a and 4a) are unfavorable for CO_2 conversion (Figs. 3c and 4c). Likewise, under the operating conditions where deactivation is relevant (that is, for low CO_2 contents in the feed), DME yield decays TOS, and conversely, CO_2 conversion increases. The effect of variables on these results is studied in more detail in section 5.

5. Use of the model for simulation

The macrokinetic model has been used for the design of the reactor, and in this case, as it quantifies the diffusion limitations, also allows predicting the behavior of the catalyst with different particle sizes.

5.1. Influence of the conditions

Fig. 5 shows the influence of pressure and temperature on DME and methanol yields and on CO_2 conversion for different CO_2/CO_x ratios in the feedstock. Although methanol is a by-product, its yield is studied for its interest as a commodity and as a raw material for selectively producing DME by dehydration. DME yield (Fig. 5a) increases with augmenting pressure, although this effect is attenuated above 50 bar. Reaction temperature also boosts DME yield up to temperatures around 300 °C, where at a maximum is observed. As to the CO_2/CO_x ratio regards, this variable is of remarkable influence and CO_2 rich feedstocks decrease significantly DME yield. In Fig. 5a a maximum value of DME yield of 64% has been achieved at 70 bar and 290 °C for syngas feeds, whereas this yield lessens to 38% under the same conditions when feeding H_2+CO_2+CO in a CO_2/

Table 2
Effective diffusion coefficients of the components through the catalyst particles.

	$D_{e,i}$ (m^2 h^{-1})
H_2	$2.6347\ 10^{-1}$
CO	$7.0393\ 10^{-2}$
CO_2	$5.6345\ 10^{-2}$
H_2O	$8.8321\ 10^{-2}$
Methanol	$5.4825\ 10^{-2}$
DME	$6.5304\ 10^{-2}$
CH_4	$9.2795\ 10^{-2}$

Table 3
Kinetic parameters of the reactions considered in the macrokinetic model.

Parameter	Value	Units
$\mathbf{k_1}^*$	1.71 10^{-5}	$mol_{Methanol}\ g^{-1}\ h^{-1}\ bar^{-3}$
$\mathbf{k_2}^*$	3.08 10^{1}	$mol_{DME}\ g^{-1}\ h^{-1}\ bar^{-2}$
$\mathbf{k_3}^*$	4.46 10^{1}	$mol\ g^{-1}\ h^{-1}\ bar^{-2}$
$\mathbf{k_4}^*$	9.23 10^{-7}	$mol_{Methanol}\ g^{-1}\ h^{-1}\ bar^{-4}$
β	1.30 10^{-3}	$mol_{HC}\ g^{-1}\ h^{-1}$
$\mathbf{E_1}$	3.84 10^{0}	kJ mol^{-1}
$\mathbf{E_2}$	2.31 10^{2}	
$\mathbf{E_3}$	9.25 10^{1}	
$\mathbf{E_4}$	8.82 10^{1}	
K^*_{ads,H_2O}	2.14 10^{0}	bar^{-1}
K^*_{ads,H_2O}	1.15 10^{-1}	
$\mathbf{\Delta H_{ads,H2O}}$	8.25 10^{-2}	kJ mol^{-1}
$\mathbf{\Delta H_{ads,CO2}}$	1.61 10^{-1}	
$\mathbf{k_d}^*$	7.50 10^{1}	$h^{-1}\ bar^{-1}$
$\mathbf{E_d}$	1.39 10^{2}	kJ mol^{-1}
d	9.38 10^{0}	
K^*_{ads,H_2O}	1.35 10^{-2}	bar^{-1}
K^*_{ads,H_2O}	1.26 10^{-2}	
$\mathbf{\Delta H^d_{ads,H2O}}$	1.02 10^{0}	kJ mol^{-1}
$\mathbf{\Delta H^d_{ads,CO2}}$	9.70 10^{-1}	

$CO_x = 0.50$ ratio, and to 17% when feeding H_2+CO_2 ($CO_2/CO_x = 1$).

Methanol yield follows the same trends as DME with increasing reaction pressure and temperature (Fig. 5b). Its yield reaches a maximum value at 70 bar and 300 °C. The influence of the content of CO_2 in the feedstock on its conversion (Fig. 5c) is opposite and less significant than that aforementioned for DME yield. In this case, increasing CO_2 concentration favors its conversion, which reaches a maximum of 32% for H_2+CO_2 feedstocks at 70 bar and 300 °C. By reducing the CO_2 content in the feed, its conversion decreases markedly, which is even negative in some operating conditions for feeds with the same CO and CO_2 content (that is, for $CO_2/CO_x = 0.50$).

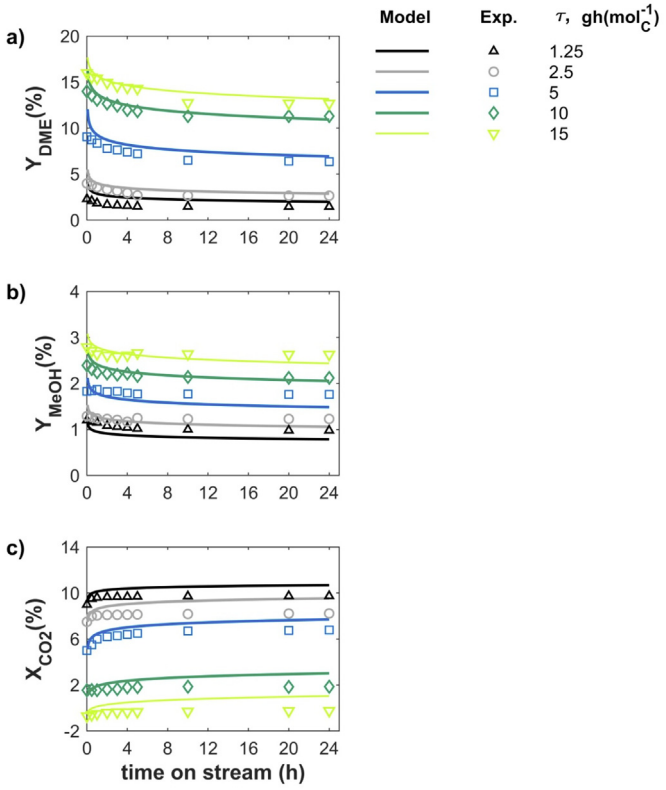

Fig. 3. Experimental results (symbols) of DME yield (a), methanol yield (b) and CO_2 conversion (c) and results obtained using the model (lines) for diverse space time values. Operating conditions: a) H_2/CO_x ratio, 3; CO_2/CO_x, 0.5; 300 °C; 30 bar.

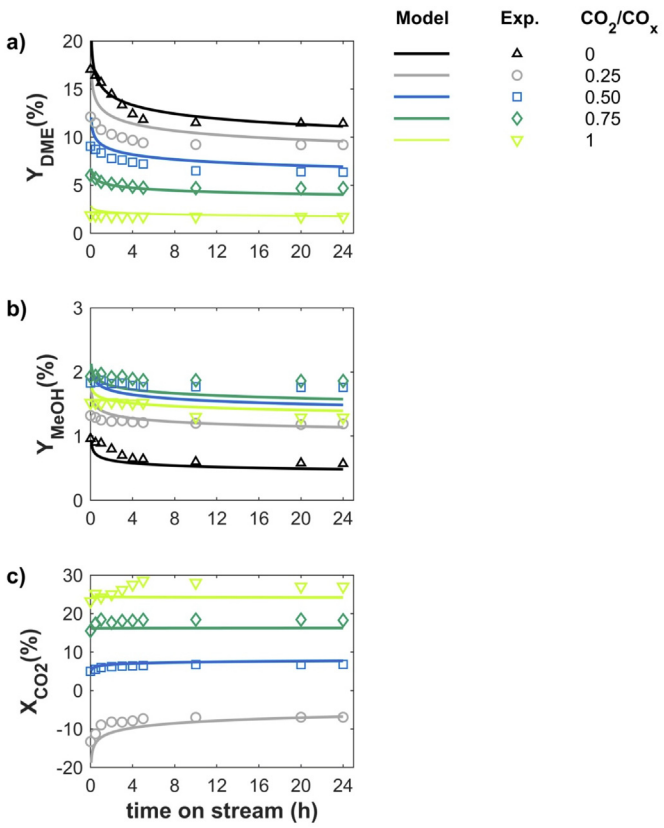

Fig. 4. Experimental results (symbols) of DME yield (a), methanol yield (b) and CO_2 conversion (c) and results obtained using the model (lines) for various CO_2/CO_X ratios. Operating conditions: a) H_2/CO_x ratio, 3; 5 g h mol_C^{-1}; 300 °C; 30 bar.

The effect of the feedstock composition on DME and methanol yields is shown in Fig. 6a for certain reaction conditions (30 bar, 300 °C, 5 g h mol_C^{-1}) selected as an example. As observed, the aforementioned effect on hampering DME yield upon increasing the CO_2content of the feedstock is remarkable. The gain in the H_2/CO_x ratio in the feedstock upturns DME yield, albeit the effect is less relevant than that resulting from diminishing CO_2/CO_x ratio, and the improvement is insignificant for values above 3.

As previously mentioned, the studied reaction has two potentially interesting objectives: i) the production of DME, due to its commercial interest; and ii) the conversion of CO_2, due to its environmental interest. Fig. 6b highlights the opposed effect of the feedstock composition on these two objectives. Thus, by increasing the content of CO_2 in the feedstock, the yield of DME decreases, but the gain in CO_2 conversion is more relevant. The increase of the H_2/CO_x ratio favors DME production and also CO_2 conversion in a greater extent.

Further information on the joint effect of the studied variables on DME and methanol yields and on CO_2 conversion for different CO_2 contents in the feed can be found in contour maps gathered in Figs. S7, S8 and S9 in the Supporting Information section.

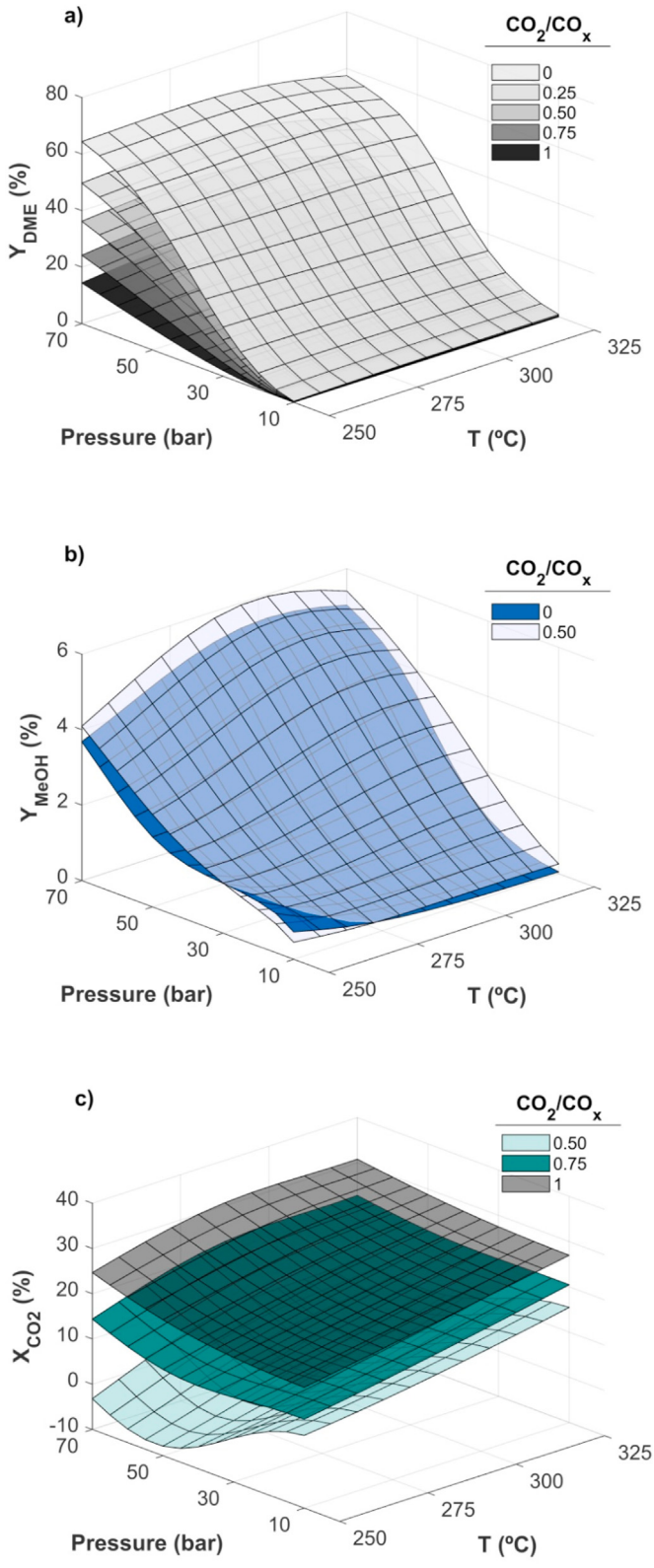

Fig. 5. Influence of temperature and pressure on DME (a) and methanol (b) yields, and on the conversion of CO_2 (c). Operating conditions: H_2/CO_x ratio, 3; 5 g h mol_C^{-1}; TOS, 1 h.

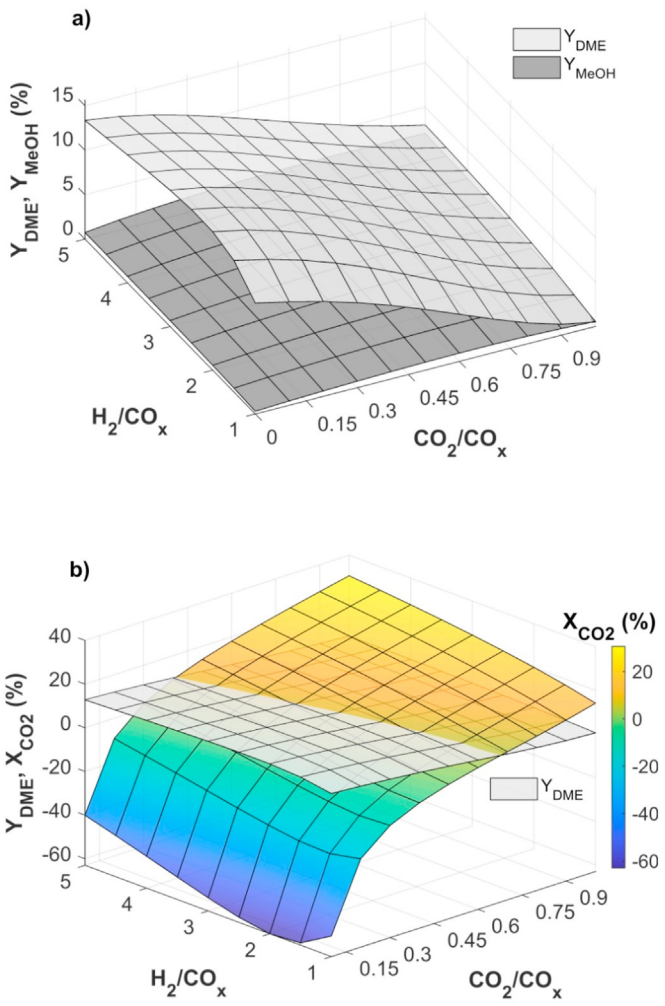

Fig. 6. Influence of the feedstock composition on DME and MeOH yields (a), and on the conversion of CO_2 (b). Operating conditions: 5 g h mol_C^{-1}; 300 °C; 30 bar; TOS, 1 h.

5.2. Influence of the catalyst particle size

The catalytic processes carried out at large scale (that is, at reactors of larger diameter) require using catalysts with larger particle size than that used here. However, particle size will affect the diffusion of the components through the catalyst according to Eq. (17). This effect has been quantified and Fig. 7 shows the incidence of particle size on the reaction indices, for certain conditions. According to these results, a moderate increase in particle diameter, up to 2 mm (4 times the size used experimentally) has small incidence on the reaction indices. Thus, DME yield decreases barely a 1% and CO_2 conversion increases by a similar magnitude.

These results are explained by the easy circulation of the components through the porous structure of the core-shell catalyst. The preparation in separate regions preserves the porous structure of each of the metallic and acid functions. This situation is different in conventional catalysts, as in this case the particles are prepared by pelletizing both functions, which reduces their porosity and as a consequence, reduces the diffusivity of the reaction medium.

It can be stated that the simulation model can be a useful tool to facilitate the preparation of core-shell catalysts. These catalysts are

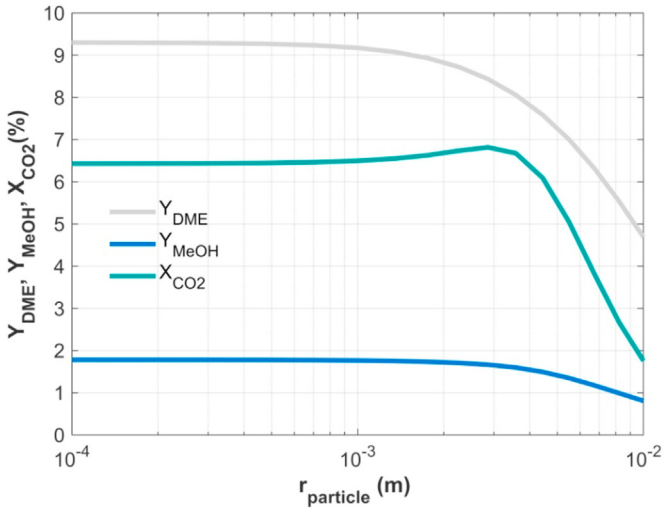

Fig. 7. Influence of catalyst particle size on DME and methanol yields and on CO_2 conversion. Operating conditions: H_2/CO_x ratio, 3; CO_2/CO_x ratio, 0.50; 5 g h mol_C^{-1}; 300 °C; 30 bar; TOS, 1 h.

a particular case of structured catalysts, whose advantages in catalytic processes are well established [67] are well established. As to the core-shell catalyst studied in this manuscript regards, it is remarkable: i) the ability to valorize CO_2 achieving higher DME yields; ii) the greater selectivity (since hydrocarbon formation side reactions are minimized) and; iii) the higher reaction temperature applicable than with conventional catalysts, giving way to a greater production of DME. These advantages are key features for the economy of the process and also to reduce its energy requirements, conditioned by the need for separating DME and recycling the reactant gases [68].

6. Conclusions

The macrokinetic model proposed to describe the reaction of DME synthesis over a CuO–ZnO–ZrO_2@SAPO-11 core-shell catalysts considers that the involved reactions occur in the different regions of the particle and quantifies the limitations of the individual reaction kinetics by diffusion constraints. The model fits accurately the experimental results obtained up to 50 bar and predicts a maximum DME yield of 64% (and 6% for byproduct methanol) at 70 bar (>45% at 50 bar) and 290 °C for syngas feeds, whereas this yield lessens to 38% under the same conditions when feeding H_2+CO/CO_2 in a CO_2/CO_x = 0.50 ratio, and to 17% when feeding H_2+CO_2 (CO_2/CO_x = 1). Higher CO_2 concentration favors its conversion, which reaches a maximum of 32% for H_2+CO_2 feedstocks at 70 bar and 300 °C, and surpasses 25% at 50 bar at that temperature.

In addition, this model allows for quantifying the influence of particle size on the reaction indices. The model predicts that increasing catalyst particle size up to 4 mm (interesting for its use in fixed bed reactors on a larger scale) has little impact on DME yield and CO_2 conversion.

Due to the characteristics of core-shell structured catalysts, the proposed kinetic model is interesting to progress in the control of the complex reaction system involved (including deactivation) and in the optimization of the properties of core-shell catalysts for this reaction. Furthermore, the basis of the model can be applied in other processes using core-shell catalysts.

CRediT authorship contribution statement

Ainara Ateka: Conceptualization, Methodology, Software, Data curation, Formal analysis, Validation, Investigation, Writing - original draft, Writing - review & editing, Visualization. **Ander Portillo:** Validation, Software, Formal analysis, Writing - original draft, Writing - review & editing. **Miguel Sánchez-Contador:** Methodology, Software, Data curation, Formal analysis, Validation, Writing - review & editing, Investigation. **Javier Bilbao:** Validation, Formal analysis, Writing - original draft, Writing - review & editing, Supervision, Project administration. **Andres T. Aguayo:** Validation, Software, Data curation, Formal analysis, Writing - original draft, Writing - review & editing, Supervision, Project administration.

Declaration of competing interest

The authors declare that they have no known competing financial interests or personal relationships that could have appeared to influence the work reported in this paper.

Acknowledgements

The following have supported the work: PID2019-108448RB-I00 of the Spanish Government, MINECO; Project IT1218-19 of the Basque Government; ERDF funds; and Contract No. 823745 (HORIZON H2020-MSCA RISE-2018) of the European Commission.

Appendix A. Supplementary data

Supplementary data to this article can be found online at https://doi.org/10.1016/j.ejphar.2021.173875.

References

[1] H. Wang, Y. Liu, A. Laaksonen, A. Krook-Riekkola, Z. Yang, X. Lu, X. Ji, Carbon recycling – an immense resource and key to a smart climate engineering: a survey of technologies, cost and impurity impact, Renew. Sustain, Energy Rev. 131 (2020), https://doi.org/10.1016/j.rser.2020.110010, 110010.
[2] I. International energy agency, world energy outlook 2019 – analysis - IEA. https://www.iea.org/reports/world-energy-outlook-2019. (Accessed 24 September 2020).
[3] R. Ahmed, G. Liu, B. Yousaf, Q. Abbas, H. Ullah, M.U. Ali, Recent advances in carbon-based renewable adsorbent for selective carbon dioxide capture and separation-A review, J. Clean. Prod. 242 (2020), 118409, https://doi.org/10.1016/j.jclepro.2019.118409.
[4] S. Zhang, Y. Zhuang, R. Tao, L. Liu, L. Zhang, J. Du, Multi-objective optimization for the deployment of carbon capture utilization and storage supply chain considering economic and environmental performance, J. Clean. Prod. 270 (2020), 122481, https://doi.org/10.1016/j.jclepro.2020.122481.
[5] A. Galadima, O. Muraza, Catalytic thermal conversion of CO_2 into fuels: perspective and challenges, Renew. Sustain. Energy Rev. 115 (2019), 109333, https://doi.org/10.1016/j.rser.2019.109333.
[6] G. Chen, G.I.N. Waterhouse, R. Shi, J. Zhao, Z. Li, L.Z. Wu, C.H. Tung, T. Zhang, From Solar Energy to Fuels: Recent Advances in Light-Driven C1 Chemistry, Angew, in: Chemie - Int (Ed.) vol. 58, 2019, pp. 17528–17551, https://doi.org/10.1002/anie.201814313.
[7] T.N. Do, J. Kim, Green C_2-C_4 hydrocarbon production through direct CO_2 hydrogenation with renewable hydrogen: process development and techno-economic analysis, Energy Convers, Manage 214 (2020), 112866, https://doi.org/10.1016/j.enconman.2020.112866.
[8] C. Panzone, R. Philippe, A. Chappaz, P. Fongarland, A. Bengaouer, Power-to-Liquid catalytic CO_2 valorization into fuels and chemicals: focus on the Fischer-Tropsch route, J. CO2 Util 38 (2020) 314–347, https://doi.org/10.1016/j.jcou.2020.02.009.
[9] A. Corma, E. Corresa, Y. Mathieu, L. Sauvanaud, S. Al-Bogami, M.S. Al-Ghrami, A. Bourane, Crude oil to chemicals: light olefins from crude oil, Catal. Sci. Technol 7 (2017) 12–46, https://doi.org/10.1039/c6cy01886f.
[10] J.N. Dedeyne, M. Geerts, P.A. Reyniers, F. Wéry, K.M. Van Geem, G.B. Marin, Computational fluid dynamics-based optimization of dimpled steam cracking reactors for reduced CO_2 emissions, AIChE J. 66 (2020), https://doi.org/10.1002/aic.16255 e16255.
[11] A. Ramirez, A. Dutta Chowdhury, M. Caglayan, A. Rodriguez-Gomez, N. Wehbe, E. Abou-Hamad, L. Gevers, S. Ould-Chikh, J. Gascon, Coated sulfated zirconia/SAPO-34 for the direct conversion of CO_2 to light olefins, Catal. Sci.

Technol 10 (2020) 1507–1517, https://doi.org/10.1039/c9cy02532d.
[12] M. Bjørgen, S. Svelle, F. Joensen, J. Nerlov, S. Kolboe, F. Bonino, L. Palumbo, S. Bordiga, U. Olsbye, Conversion of methanol to hydrocarbons over zeolite H-ZSM-5: on the origin of the olefinic species, J. Catal. 249 (2007) 195–207, https://doi.org/10.1016/j.jcat.2007.04.006.
[13] Y. An, T. Lin, F. Yu, Y. Yang, L. Zhong, M. Wu, Y. Sun, Advances in direct production of value-added chemicals via syngas conversion, Sci. China Chem. 60 (2017) 887–903, https://doi.org/10.1007/s11426-016-0464-1.
[14] G. Wang, L. Zeng, J. Cao, F. Liu, Q. Lin, Y. Yi, H. Pan, Highly selective conversion of CO_2 to hydrocarbons over composite catalysts of ZnO-ZrO_2 and SAPO-34, Microporous Mesoporous Mater. 284 (2019) 133–140, https://doi.org/10.1016/j.micromeso.2019.04.023.
[15] G. Wang, Y. Wang, J. Cao, X. Wang, Y. Yi, F. Liu, Fabrication of $ZnZrO_2$@Al_2O_3@SAPO-34 tandem catalyst for CO_2 conversion to hydrocarbons, Microporous Mesoporous Mater. 291 (2020), https://doi.org/10.1016/j.micromeso.2019.109693, 109693.
[16] M. Sedighi, M. Mohammadi, CO_2 hydrogenation to light olefins over Cu-CeO_2/SAPO-34 catalysts: product distribution and optimization, J. CO2 Util 35 (2020) 236–244, https://doi.org/10.1016/j.jcou.2019.10.002.
[17] C. Zhou, J. Shi, W. Zhou, K. Cheng, Q. Zhang, J. Kang, Y. Wang, Highly active ZnO-ZrO_2 aerogels integrated with H-ZSM-5 for aromatics synthesis from carbon dioxide, ACS Catal. 10 (2020) 302–310, https://doi.org/10.1021/acscatal.9b04309.
[18] G.A. Olah, A. Goeppert, G.K.S. Prakash, Chemical recycling of carbon dioxide to methanol and dimethyl ether: from greenhouse gas to renewable, environmentally carbon neutral fuels and synthetic hydrocarbons, J. Org. Chem. 74 (2009) 487–498, https://doi.org/10.1021/jo801260f.
[19] S. Michailos, S. McCord, V. Sick, G. Stokes, P. Styring, Dimethyl ether synthesis via captured CO_2 hydrogenation within the power to liquids concept: a techno-economic assessment, Energy Convers, Manage 184 (2019) 262–276, https://doi.org/10.1016/j.enconman.2019.01.046.
[20] K. Saravanan, H. Ham, N. Tsubaki, J.W. Bae, Recent progress for direct synthesis of dimethyl ether from syngas on the heterogeneous bifunctional hybrid catalysts, Appl. Catal. B Environ. 217 (2017) 494–522, https://doi.org/10.1016/j.apcatb.2017.05.085.
[21] E. Catizzone, G. Bonura, M. Migliori, F. Frusteri, G. Giordano, CO_2 recycling to dimethyl ether: state-of-the-art and perspectives, Molecules 23 (2018) 31–59, https://doi.org/10.3390/molecules23010031.
[22] U. Mondal, G.D. Yadav, Perspective of dimethyl ether as fuel: Part I. Catalysis, J. CO2 Util 32 (2019) 299–320, https://doi.org/10.1016/j.jcou.2019.02.003.
[23] U. Mondal, G.D. Yadav, Perspective of dimethyl ether as fuel_ Part II- analysis of reactor systems and industrial processes, J. CO2 Util 32 (2019) 321–338, https://doi.org/10.1016/j.jcou.2019.02.006.
[24] A. Ateka, J. Ereña, J. Bilbao, A.T. Aguayo, Strategies for the intensification of CO_2 valorization in the one-step dimethyl ether synthesis process, Ind. Eng. Chem. Res. 59 (2020) 713–722, https://doi.org/10.1021/acs.iecr.9b05749.
[25] M. De Falco, M. Capocelli, G. Centi, Dimethyl ether production from CO_2 rich feedstocks in a one-step process: thermodynamic evaluation and reactor simulation, Chem. Eng. J. 294 (2016) 400–409, https://doi.org/10.1016/j.cej.2016.03.009.
[26] A. Ateka, P. Pérez-Uriarte, M. Gamero, J. Ereña, A.T. Aguayo, J. Bilbao, A comparative thermodynamic study on the CO_2 conversion in the synthesis of methanol and of DME,, Energy 120 (2017) 796–804, https://doi.org/10.1016/j.energy.2016.11.129.
[27] L. Kubelkova, J. Nova kova, K. Nedomova, Reactivity of surface species on zeolites in methanol conversion, J. Catal. 124 (1990) 441–450, https://doi.org/10.1016/0021-9517(90)90191-l.
[28] S.R. Blaszkowski, R.A. van Santen, The mechanism of dimethyl ether formation from methanol catalyzed by zeolitic protons,, J. Am. Chem. Soc. 118 (1996) 5152–5153, https://doi.org/10.1021/ja954323k.
[29] A. Ghorbanpour, J.D. Rimer, L.C. Grabow, Computational assessment of the dominant factors governing the mechanism of methanol dehydration over H-ZSM-5 with heterogeneous aluminum distribution, ACS Catal. 6 (2016) 2287–2298, https://doi.org/10.1021/acscatal.5b02367.
[30] C. Arcoumanis, C. Bae, R. Crookes, E. Kinoshita, The potential of di-methyl ether (DME) as an alternative fuel for compression-ignition engines: a review,, Fuel 87 (2008) 1014–1030, https://doi.org/10.1016/j.fuel.2007.06.007.
[31] D. Kim, B. Choi, G. Park, K. Lee, D.W. Lee, S. Jung, Effect of γ-Al_2O_3 characteristics on hydrogen production of Cu/γ-Al_2O_3 catalyst for steam reforming of dimethyl ether, Chem. Eng. Sci. 216 (2020), https://doi.org/10.1016/j.ces.2020.115535, 115535.
[32] P. Pérez-Uriarte, A. Ateka, M. Gamero, A.T. Aguayo, J. Bilbao, Effect of the operating conditions in the transformation of DME to olefins over a HZSM-5 zeolite catalyst, Ind. Eng. Chem. Res. 55 (2016) 6569–6578, https://doi.org/10.1021/acs.iecr.6b00627.
[33] T. Cordero-Lanzac, A. Ateka, P. Pérez-Uriarte, P. Castaño, A.T. Aguayo, J. Bilbao, Insight into the deactivation and regeneration of HZSM-5 zeolite catalysts in the conversion of dimethyl ether to olefins, Ind. Eng. Chem. Res. 57 (2018) 13689–13702, https://doi.org/10.1021/acs.iecr.8b03308.
[34] N.N. Ezhova, N.V. Kolesnichenko, T.I. Batova, Zeolite catalysts for the synthesis of lower olefins from dimethyl ether (a Review), Petrol. Chem. 60 (2020) 459–470, https://doi.org/10.1134/S0965544120040064.
[35] T. Cordero-Lanzac, A.T. Aguayo, J. Bilbao, Reactor–regenerator system for the dimethyl ether-to-olefins process over HZSM-5 catalysts: conceptual development and analysis of the process variables, Ind. Eng. Chem. Res. 59 (2020) 14689–14702, https://doi.org/10.1021/acs.iecr.0c02276.
[36] J. Sun, G. Yang, Y. Yoneyama, N. Tsubaki, Catalysis chemistry of dimethyl ether synthesis, ACS Catal. 4 (2014) 3346–3356, https://doi.org/10.1021/cs500967j.
[37] G. Bonura, M. Cordaro, C. Cannilla, A. Mezzapica, L. Spadaro, F. Arena, F. Frusteri, Catalytic behaviour of a bifunctional system for the one step synthesis of DME by CO_2 hydrogenation, Catal. Today 228 (2014) 51–57, https://doi.org/10.1016/j.cattod.2013.11.017.
[38] M. Cai, V. Subramanian, V. V Sushkevich, V. V Ordomsky, A.Y. Khodakov, Effect of Sn additives on the CuZnAl–HZSM-5 hybrid catalysts for the direct DME synthesis from syngas, Appl. Catal. Gen. 502 (2015) 370–379, https://doi.org/10.1016/j.apcata.2015.06.030.
[39] F. Frusteri, G. Bonura, C. Cannilla, G. Drago Ferrante, A. Aloise, E. Catizzone, M. Migliori, G. Giordano, Stepwise tuning of metal-oxide and acid sites of CuZnZr-MFI hybrid catalysts for the direct DME synthesis by CO_2 hydrogenation, Appl. Catal, B Environ (2015) 522–531, https://doi.org/10.1016/j.apcatb.2015.04.032, 176–177.
[40] S. Asthana, C. Samanta, A. Bhaumik, B. Banerjee, R.K. Voolapalli, B. Saha, Direct synthesis of dimethyl ether from syngas over Cu-based catalysts: enhanced selectivity in the presence of MgO, J. Catal. 334 (2016) 89–101, https://doi.org/10.1016/j.jcat.2015.10.020.
[41] A. Ateka, I. Sierra, J. Ereña, J. Bilbao, A.T. Aguayo, Performance of CuO–ZnO–ZrO_2 and CuO–ZnO–MnO as metallic functions and SAPO-18 as acid function of the catalyst for the synthesis of DME co-feeding CO_2, Fuel Process, Technol. 152 (2016) 34–45, https://doi.org/10.1016/j.fuproc.2016.05.041.
[42] Z. Qin, X. Zhou, T. Su, Y. Jiang, H. Ji, Hydrogenation of CO_2 to dimethyl ether on La-, Ce-modified Cu-Fe/HZSM-5 catalysts, Catal. Commun. 75 (2016) 78–82, https://doi.org/10.1016/j.catcom.2015.12.010.
[43] X. Zhou, T. Su, Y. Jiang, Z. Qin, H. Ji, Z. Guo, CuO-Fe_2O_3-CeO_2/HZSM-5 bifunctional catalyst hydrogenated CO_2 for enhanced dimethyl ether synthesis, Chem. Eng. Sci. 153 (2016) 10–20, https://doi.org/10.1016/j.ces.2016.07.007.
[44] G. Bonura, M. Migliori, L. Frusteri, C. Cannilla, E. Catizzone, G. Giordano, F. Frusteri, Acidity control of zeolite functionality on activity and stability of hybrid catalysts during DME production via CO_2 hydrogenation, J. CO2 Util 24 (2018) 398–406, https://doi.org/10.1016/j.jcou.2018.01.028.
[45] M. Cai, A. Palčić, V. Subramanian, S. Moldovan, O. Ersen, V. Valtchev, V. V Ordomsky, A.Y. Khodakov, Direct dimethyl ether synthesis from syngas on copper–zeolite hybrid catalysts with a wide range of zeolite particle sizes, J. Catal. 338 (2016) 227–238, https://doi.org/10.1016/j.jcat.2016.02.025.
[46] A.T. Aguayo, J. Ereña, I. Sierra, M. Olazar, J. Bilbao, Deactivation and regeneration of hybrid catalysts in the single-step synthesis of dimethyl ether from syngas and CO_2, Catal. Today 106 (2005) 265–270, https://doi.org/10.1016/j.cattod.2005.07.144.
[47] J. Ereña, I. Sierra, A.T. Aguayo, A. Ateka, M. Olazar, J. Bilbao, Kinetic modelling of dimethyl ether synthesis from (H_2+CO_2) by considering catalyst deactivation, Chem. Eng. J. 174 (2011) 660–667, https://doi.org/10.1016/j.cej.2011.09.067.
[48] I. Sierra, J. Ereña, A.T. Aguayo, J.M. Arandes, M. Olazar, J. Bilbao, Co-feeding water to attenuate deactivation of the catalyst metallic function (CuO–ZnO–Al_2O_3) by coke in the direct synthesis of dimethyl ether, Appl. Catal. B Environ. 106 (2011) 167–173, https://doi.org/10.1016/j.apcatb.2011.05.021.
[49] M. Sánchez-Contador, A. Ateka, A.T. Aguayo, J. Bilbao, Direct synthesis of dimethyl ether from CO and CO_2 over a core-shell structured CuO-ZnO-ZrO_2@SAPO-11 catalyst, Fuel Process, Technol. 179 (2018) 258–268, https://doi.org/10.1016/j.fuproc.2018.07.009.
[50] M. Sánchez-Contador, A. Ateka, M. Ibáñez, J. Bilbao, A.T. Aguayo, Influence of the operating conditions on the behavior and deactivation of a CuO-ZnO-ZrO_2@SAPO-11 core-shell-like catalyst in the direct synthesis of DME, Renew. Energy 138 (2019) 585–597, https://doi.org/10.1016/j.renene.2019.01.093.
[51] M. Sánchez-Contador, A. Ateka, P. Rodriguez-Vega, J. Bilbao, A.T. Aguayo, Optimization of the Zr content in the CuO-ZnO-ZrO_2/SAPO-11 catalyst for the selective hydrogenation of CO+CO_2 mixtures in the direct synthesis of dimethyl ether, Ind. Eng. Chem. Res. 57 (2018) 1169–1178, https://doi.org/10.1021/acs.iecr.7b04345.
[52] M. Sánchez-Contador, A. Ateka, A.T. Aguayo, J. Bilbao, Behavior of SAPO-11 as acid function in the direct synthesis of dimethyl ether from syngas and CO_2, J. Ind. Eng. Chem. 63 (2018) 245–254, https://doi.org/10.1016/j.jiec.2018.02.022.
[53] A. Ateka, M. Sánchez-Contador, A. Portillo, J. Bilbao, A.T. Aguayo, Kinetic modeling of CO_2+CO hydrogenation to DME over a CuO-ZnO-ZrO_2@SAPO-11 core-shell catalyst, Fuel Process, Technol. 206 (2020) 106434–106444, https://doi.org/10.1016/j.fuproc.2020.106434.
[54] K. Pinkaew, G. Yang, T. Vitidsant, Y. Jin, C. Zeng, Y. Yoneyama, N. Tsubaki, A new core–shell-like capsule catalyst with SAPO-46 zeolite shell encapsulated Cr/ZnO for the controlled tandem synthesis of dimethyl ether from syngas,, Fuel 111 (2013) 727–732, https://doi.org/10.1016/j.fuel.2013.03.027.
[55] Y. Wang, W. Wang, Y. Chen, J. Ma, R. Li, Synthesis of dimethyl ether from syngas over core–shell structure catalyst CuO–ZnO–Al_2O_3@SiO_2–Al_2O_3, Chem. Eng. J. 250 (2014) 248–256, https://doi.org/10.1016/j.cej.2014.04.018.
[56] R. Phienluphon, K. Pinkaew, G. Yang, J. Li, Q. Wei, Y. Yoneyama, T. Vitidsant, N. Tsubaki, Designing core (Cu/ZnO/Al_2O_3)–shell (SAPO-11) zeolite capsule catalyst with a facile physical way for dimethyl ether direct synthesis from syngas, Chem. Eng. J. 270 (2015) 605–611, https://doi.org/10.1016/j.cej.2015.02.071.
[57] S. Das, J. Pérez-Ramírez, J. Gong, N. Dewangan, K. Hidajat, B.C. Gates, S. Kawi, Core-shell structured catalysts for thermocatalytic, photocatalytic, and

electrocatalytic conversion of CO_2, Chem. Soc. Rev. 49 (2020) 2937–3004, https://doi.org/10.1039/c9cs00713j.
[58] P.B. Weisz, J.S. Hicks, The behaviour of porous catalyst particles in view of internal mass and heat diffusion effects,, Chem. Eng. Sci. 50 (1995) 3951–3958, https://doi.org/10.1016/0009-2509(96)81827-6.
[59] K.B. Bischoff, Effectiveness factors for general reaction rate forms, AIChE J. 11 (1965) 351–355, https://doi.org/10.1002/aic.690110229.
[60] H.W. Haynes, An explicit approximation for the effectiveness factor in porous heterogeneous catalysts, Chem. Eng. Sci. 41 (1986) 412–415, https://doi.org/10.1016/0009-2509(86)87022-1.
[61] E. Magyari, Exact analytical solutions of diffusion reaction in spherical porous catalyst, Chem. Eng. J. 158 (2010) 266–270, https://doi.org/10.1016/j.cej.2010.01.034.
[62] H.S. Fogler, Elements of Chemical Reaction Engineering, Prentice Hall, Pennsylvania, USA, 2005.
[63] A.T. Aguayo, J. Ereña, D. Mier, J.M. Arandes, M. Olazar, J. Bilbao, Kinetic modeling of dimethyl ether synthesis in a single step on a CuO-ZnO-Al_2O_3/γ-Al_2O_3 catalyst, Ind. Eng. Chem. Res. 46 (2007) 5522–5530, https://doi.org/10.1021/ie070269s.
[64] A. García-Trenco, A. Vidal-Moya, A. Martínez, Study of the interaction between components in hybrid CuZnAl/HZSM-5 catalysts and its impact in the syngas-to-DME reaction, Catal. Today 179 (2012) 43–51, https://doi.org/10.1016/j.cattod.2011.06.034.
[65] G. Bonura, C. Cannilla, L. Frusteri, E. Catizzone, S. Todaro, M. Migliori, G. Giordano, F. Frusteri, Interaction effects between CuO-ZnO-ZrO_2 methanol phase and zeolite surface affecting stability of hybrid systems during one-step CO_2 hydrogenation to DME, Catal. Today 345 (2020) 175–182, https://doi.org/10.1016/j.cattod.2019.08.014.
[66] M. Migliori, A. Condello, F. Dalena, E. Catizzone, G. Giordano, CuZnZr-zeolite hybrid grains for DME synthesis: new evidence on the role of metal-acidic features on the methanol conversion step, Catalysts 10 (2020) 671, https://doi.org/10.3390/catal10060671.
[67] F. Kapteijn, J.A.Moulijn, Structured Catalysts and Reactors – Perspectives for Demanding Applications, Catal. Today, in Press. doi: 10.1016/j.cattod.2020.09.026.
[68] C. Mevawalaa, Y. Jiangb, D. Bhattacharyyaa, Techno-economic optimization of shale gas to dimethyl ether production processes via direct and indirect synthesis routes, Appl. Energy 238 (2019) 119–134, https://doi.org/10.1016/j.apenergy.2019.01.044.